Soft Matter

ROYAL SOCIETY OF CHEMISTRY

PAPER

View Article Online
View Journal | View Issue

Cite this: *Soft Matter*, 2024, **20**, 4608

Charged hollow microgel capsules†

Nabanita Hazra, Janik Lammertz, Andrey Babenyshev, Rebecca Erkes,
Fabian Hagemans, Chandeshwar Misra, Walter Richtering and
Jérôme J. Crassous *

Responsive hollow microgels are a fascinating class of soft model systems at the crossover between polymer capsules and microgels. The presence of the cavity makes them promising materials for encapsulation and controlled release applications but also confers them an additional softness that is reflected by their peculiar behaviour in bulk and at interfaces. Their responsivity to external stimuli, such as temperature, pH, and ionic strength, can be designed from their synthesis conditions and the choice of functional moieties. So far most studies have focused on "small" hollow microgels that were mostly studied with scattering or atomic force microscopy techniques. In our previous study, we have shown that large fluorescent hollow poly(*N*-isopropylacrylamide) (PNIPAM) microgels could be synthesized using micrometer-sized silica particles as sacrificial templates allowing their investigation *in situ via* confocal microscopy. In this work, we extend this approach to charged large hollow microgels based on poly(*N*-isopropylacrylamide-*co*-itaconic acid) (P(NIPAM-*co*-IA)). Hereby, we compare the structure and responsivity of "neutral" (PNIPAM) and "charged" (P(NIPAM-*co*-IA)) hollow microgel systems synthesized under similar conditions with the same sacrificial template using confocal and atomic force microscopy and light scattering techniques. In particular, we could demonstrate the extremely soft character of the swollen charged hollow microgels and their responsivity to pH, ionic strength, and temperature. To conclude this study, the buckling behavior of the different capsules was investigated illustrating the potential of such systems to change its conformation by varying the osmotic pressure and pH conditions.

Received 24th January 2024,
Accepted 13th May 2024

DOI: 10.1039/d4sm00111g

rsc.li/soft-matter-journal

Microgels are cross-linked polymer networks typically swollen in a good solvent, such as water, and formed a three-dimensional macromolecular network with a colloidal size range.[1,2] Microgels combine classic characteristics of polymers, colloids, and surfactants.[3,4] That is, they are soft and porous, crystallize depending on concentration, and adsorb at interfaces since they lower the interfacial tension. The softness enables swelling, deformation, and interpenetration of microgels upon the influence of forces.[1,5] In addition, microgels show swelling and deswelling behavior towards multiple external stimuli, such as temperature,[2,6,7] pH,[8–12] and ionic strength.[13] Stimuli responsivity and softness make microgels appealing for industrial applications, such as catalysis[14] or purification technology,[15] but also for biomedical applications as biosensors,[16,17] implant coatings[18] or drug delivery systems.[19–22] Advantageously, microgel properties can be adjusted to a great extent by changing their chemical composition or architecture.[3,23,24]

Hollow sensitive microgels provide promising characteristics and have been investigated in the past decades.[25,26] They have a solvent-filled cavity that offers additional freedom for the expansion of the polymer chains and affects their mechanical behavior.[27–30] Due to the cavity, hollow microgels are ideal as carriers with a high capacity for small species compared to conventional microgels.[31–33] Particularly, (multi-)stimuli sensitivity enables controlled uptake and release of the guest species.[34–37] Encapsulation and release may be triggered both by changing the network density[38] and by changing the interactions between guest species and the microgel network.[11,39] In previous studies, the preparation of poly(*N*-isopropylacrylamide) (PNIPAM) based nano/microcapsules has been achieved *via* various synthetic pathways, including semi-batch and temperature-programmed surfactant-free precipitation polymerization,[40] inverse emulsion[41,42] and miniemulsion[43,44] polymerization, and layer-by-layer (LbL) assembly and click chemistry techniques.[45] Among the different synthetic approaches, seed emulsion polymerization using a sacrificial polymeric core[25,46] or inorganic silica core[5,26,27,47]

Institute of Physical Chemistry, RWTH Aachen University, Landoltweg 2, 52074, Aachen, Germany. E-mail: crassous@pc.rwth-aachen.de

† Electronic supplementary information (ESI) available. See DOI: https://doi.org/10.1039/d4sm00111g

have been extensively applied for the creation of diverse PNIPAM based hollow microgels. Lapeyre *et al.*,[47] Dubbert *et al.*[48] and more recently Brugnoni *et al.*[49] investigated hollow double-shell microgels with diameters of a few hundred nanometers. Lapeyre *et al.* demonstrated the multi-responsive character of their hollow microgels with an inner layer of PNIPMAM and an outer layer of PNIPAM copolymerized with either acrylic acid (AA) or phenylboronic acid (PBA) to implement an additional responsiveness toward pH or glucose, respectively.[47] While Dubbert *et al.* utilized an inner shell of poly(*N*-isopropylacrylamide) (PNIPAM) and an outer shell of poly(*N*-isopropylmethacrylamide) (PNIPMAM), Brugnoni *et al.* employed an inner shell of poly(*N*-isopropylacrylamide-*co*-diacetone acrylamide) (P(NIPAM-*co*-DAAM)) and an outer shell of PNIPAM. In both cases, the inner and outer shells exhibit different temperature sensitivities, which may be used to tailor the temperature-triggered uptake and release of the guest species.

In addition, Wypysek *et al.*[50] used hollow microgels based on poly(*N*-isopropylacrylamide-*co*-itaconic acid) (P(NIPAM-*co*-IA)) with a diameter of a few hundred nanometers. The microgels are neutral at low pH values and negatively charged at high pH values due to deprotonation of the acidic group. The neutral microgels are mainly sensitive to temperature changes whereas the charged microgels are mainly sensitive to changes in ionic strength. Hollow microgels possess exceptional architecture and morphology, making them particularly valuable for encapsulating sensitive molecules like enzymes and proteins, as well as entrapping toxins and bioactive molecules. In a recent work of Wypysek *et al.*[33] they synthesized hollow polyelectrolyte anionic P(*N*-isopropylacrylamide-*co*-itaconic acid) microgels and investigated their encapsulation behaviour as nanocontainers for the model protein cytochrome *c* as a function of pH. They employed fluorescence-lifetime imaging (FLIM) to determine the spatial distribution of the protein within the hollow microgels. Their findings elucidated how pH fluctuations, from low to high levels, affected the protein's electrostatic interactions within the microgels, alternating between no interaction, attraction, and repulsion.[33]

Hollow microgels are distinguished by the relative size of shell thickness and radius. Additionally, hollow microgels with a thin shell in comparison to the cavity are comparable to microcapsules and might exhibit different mechanical behavior.[51] We note however, that most of the hollow microgels based on a silica sacrificial template produced so far use a core of only a few hundred nanometers in diameter. In our previous work, we described the synthesis and characterization of highly monodisperse micron-sized hollow PNIPAM microgels with relatively thin shells and temperature sensitivity.[52] This capsule size is optimal to determine accurately the system dimensions using light scattering techniques and for *in situ* imaging by using confocal fluorescence microscopy when the polymer network is labelled. The capsules were found to deform when exposed to an external osmotic pressure induced by the addition of free polymers in the bulk solution. It was demonstrated that high molecular weight dextran macromolecules were apparently hindered from entering the cavity. Exceeding a critical osmotic pressure, the capsules buckle. According to the theory of elasticity,[53] the Youngs modulus of the capsules was determined from the critical buckling osmotic pressure.

In the present study, we extend the synthesis of such micrometric hollow microgel capsules to charged microgel capsules. Starting with the same silica core particles as templates, two synthesis routes are described leading to well-defined and monodisperse "neutral" PNIPAM hollow microgel capsules and "charged" P(NIPAM-*co*-IA) hollow microgel capsules. We present the characterization of these two systems based on different scattering and microscopy techniques. The pH dependence of the P(NIPAM-*co*-IA) hollow microgel capsules was further tested confirming the extended swelling of the network under low pH conditions. Such particles were found to be much softer than their neutral analogues, which was confirmed by their high deformation when adsorbed at a solid substrate, using atomic force microscopy. Finally, the buckling of PNIPAM and P(NIPAM-*co*-IA) microgel capsules at high osmotic pressure set by the addition of high molecular weight dextran was investigated under different pH conditions.

1 Materials and methods

Materials

3-Aminopropyl triethoxysilane (APTES, Fluka), tetraethyl orthosilicate (TEOS, Sigma-Aldrich), ethanol absolute (absolute EtOH, VWR Chemicals), ammonium hydroxide solution (Amonia, Merck) fluorescein isothiocyanate isomer I (FITC, Sigma Aldrich), 3-(Trimethoxysilyl)propylmethacrylate (MPS, AppliChem), *N*-isopropylacrylamide (NIPAM, Acros Organics), *N*,*N*′-methylenebisacrylamide (BIS, Sigma-Aldrich), potassium peroxodisulfate (KPS, Fluka), dimethyl itaconate (DMI, Sigma-Aldrich), methacryloxyethyl thiocarbamoyl rhodamine B (MRB, Polysciences, Inc.) and sodium hydroxide (NaOH, Alfa Aesar) were used as received.

Synthesis

The synthesis of micro-sized responsive capsules was executed in four steps as schematically depicted in Fig. 1. In the first step, silica templates were generated through a semi-continuous Stöber method. In doing so, seed concentration and other factors were varied to approximate the appropriate particle size and polydispersity. In the second step, the surface of the silica template was modified. In the third step, a precipitation polymerization with either NIPAM and BIS or DMI, NIPAM and BIS, together with the fluorescent dye MRB, was performed in order to produce labelled core–shell particles. The neutral monomer DMI was chosen because it does not reduce the colloidal stability and can be saponified to itaconic acid (IA) in contrast to charged monomers. In the fourth step, the silica cores were dissolved in NaOH solution and the charged microcapsules were obtained.

Synthesis of silica templates. First, small, labelled silica seeds were synthesized using the Stöber method.[54] Therefore,

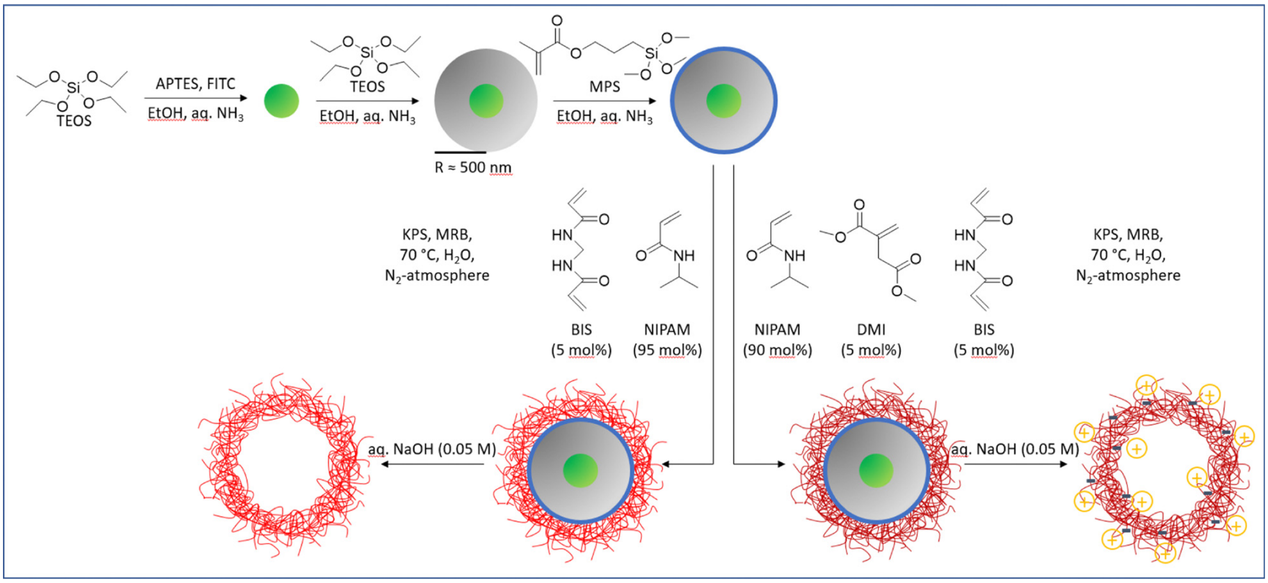

Fig. 1 Schematic four-step synthesis of microgel capsules, including preparation of silica templates, modification of silica surface, microgel shell polymerization, and silica core dissolution.

49 mg FITC (0.13 mmol) were dissolved in 2 mL absolute EtOH. After the addition of 0.300 μL APTES (1.29 mmol), the solution was stirred in the dark for 3 h. 34 mL ammonia (26.1%) and 330 mL absolute EtOH were mixed in a single neck round bottom flask. The prepared solutions of labelled APTES and 14 mL TEOS (63.17 mmol) were simultaneously and quickly added while stirring vigorously. After approximately 20 min and arising turbidity, the stirring speed was reduced, and the solution was stirred at a moderate level in the dark for a further 48 h. The silica seeds were purified and separated by several centrifugation and washing steps with absolute EtOH. Afterwards, the small, labelled silica seeds were grown into micro-sized silica particles by using a semi-continuous Stöber method.[54] The silica seeds were stirred for several days and sonicated for 60 min immediately before application to avoid aggregation. A mixture of silica seeds in absolute EtOH with a total volume of 67.8 mL and a mass concentration of 2.68 mg mL^{-1} by a particle radius of 179 ± 10 nm was prepared in a single neck round bottom flask and sonicated for a further 60 min. 8.9 mL double distilled water and 3.6 mL ammonia (26.1%) were added to the solution while stirring. Two mixtures were prepared. The first consisted of 20 mL TEOS (90.25 mmol) and 40 mL absolute EtOH to maintain a constant TEOS concentration. The second contained 41.3 mL absolute EtOH, 13.3 mL bidistilled water, and 5.4 mL ammonia (26.1%) to balance the change in pH value. Both mixtures were added simultaneously *via* a syringe pump with a flow rate of 0.5 mL h^{-1} to the vigorously stirred silica seed solution. After complete addition, the mixture was stirred for a further 24 h. The silica particles were purified and separated by ten centrifugation cycles and washing steps with absolute EtOH until the supernatant was clear.

Surface modification of silica templates. In the second step, the silica particles were functionalized by surface modification with MPS to facilitate the precipitation polymerization in the third step by introducing polymerizable double bonds to the particle surface. Thus, the silica particles were stirred for several days and sonicated for 60 min immediately before use in order to avoid aggregation. A mixture of silica particles in absolute EtOH with a total volume of 109.6 mL and a mass concentration of 9.43 mg mL^{-1} with a particle radius of 538 ± 45 nm was prepared in a single neck round bottom flask and sonicated for a further 60 min. Afterwards, 30.8 mL of ammonia (26.1%) was added and 3.34 g MPS (13.4 mmol) was dropwise added to the mixture over a time range of 2 h while stirring. Following the overnight stirring, the mixture was heated to 75 °C for 1 hour and then cooled down to room temperature. The modified silica particles were purified by three centrifugation runs and washing with absolute EtOH. Afterwards, the solvent was exchanged by three more centrifugation runs and washing with bidistilled water.

Synthesis of core–shell silica/PNIPAM microgels. A mixture of rhodamine B methacrylate in filtered double distilled water was prepared with a concentration of 1 mg mL^{-1} and stirred for at least one day. The synthesis was performed in a three neck 250 mL round bottom flask equipped with a reflux condenser, a magnetic stirrer, and two rubber septa. The nitrogen inlet was placed in the flask whereas the temperature sensor was placed in the oil bath. 1053.0 mg NIPAM (9.305 mmol, 94 mol%), 76.0 mg BIS (0.493 mmol, 5 mol%) and 17.4 mg KPS (0.064 mmol, 1 mol%) were dissolved in filtered double distilled water. 1.07 mL dye solution (0.0016 mmol) was added to the flask. Modified silica solution and double distilled water were added to a volume of 193 mL and a silica mass concentration of 2.672 mg mL^{-1} with a particle radius of 538 ± 45 nm. The solution was degassed for 60 min. The reaction was started by placing the flask in a preheated oil bath at 70 °C and proceeded for 3 h under a nitrogen atmosphere.

Afterwards, the mixture was gently stirred and cooled to room temperature.

Synthesis of core–shell silica/P(NIPAM-*co*-DMI) microgels. Due to colloidal stability, the uncharged comonomer DMI was chosen over charged monomers. DMI offers the possibility for post-modification in the fourth step by generating charged IA groups.[50] 997.5 mg NIPAM (8.815 mmol, 89 mol%), 77.50 mg DMI (0.490 mmol, 5 mol%), 76.30 mg BIS (0.495 mmol, 5 mol%), and 17.8 mg KPS (0.066 mmol, 1 mol%) were dissolved in filtered double distilled water. 1.07 mL dye solution (0.0016 mmol) was added to the flask. Modified silica solution and double distilled water were added to a volume of 193 mL and a silica mass concentration of 2.672 mg mL^{-1} with a particle radius of 538 ± 45 nm. The solution was degassed for 60 min. The reaction was started by placing the flask in a preheated oil bath at 70 °C and proceeded for 3 h under a nitrogen atmosphere. Afterwards, the mixture was cooled down to room temperature. The solutions were purified and small regular microgels were separated by centrifugation and washing with Milli-Q-water until the supernatant was clear.

Generation of hollow microgels. In the fourth step, microgel capsules were produced from the core–shell particles by dissolution of the silica core in NaOH solution. Thus, the volume of the core–shell particle mixture was reduced to 10 mL by centrifugation. 5 mL of the mixture was transferred to 50 mL NaOH solution (0.05 M) and mixed on a roller plate for three days. Afterwards, the mixture was dialysed against NaOH solution (0.05 M, MWCO 12–14 kDa, 50 mL inner volume *vs.* 750 mL outer volume) for at least 10 days. Finally, the NaOH solution was replaced by dialysis against Milli-Q-water.

Buffer preparation. For the characterization of the charged microgel capsules, buffers with varying pH values and ionic strength were used. For the sample preparation in general, 0.25 mL microgel solution was mixed with 2.5 mL buffer solution. In addition, another two sets of the charged microgel capsules with glycine buffers with different pH values were prepared by mixing 0.667 mL of the stock solution of hollow P(NIPAM-*co*-IA) capsules and 3.333 mL of the buffer solution to obtain a concentration of 0.0035 wt%.

Glycine/HCl buffer (5 mM, pH = 3, I = 1 mM). The buffer was prepared by dissolving 37.53 mg glycine in approximately 70 mL double distilled water. Afterwards, 0.898 mL HCl solution (0.1 M) was added and the volume was filled up to 100 mL with double distilled water. Finally, the pH value was adjusted with NaOH solution (0.1 M) or HCl solution (0.1 M).

Glycine/HCl buffer (5 mM, pH = 3, I = 10 mM). The buffer was prepared by dissolving 37.53 mg glycine and 53.19 mg NaCl in approximately 70 mL double distilled water. Subsequently, 0.898 mL HCl solution (0.1 M) was added and the volume was filled up to 100 mL with double distilled water. Finally, the pH value was adjusted with NaOH solution (0.1 M) or HCl solution (0.1 M).

Glycine/NaOH buffer (5 mM, pH = 9, I = 1 mM). The buffer was prepared by dissolving 37.53 mg glycine in approximately 70 mL double distilled water. Afterwards, 1.041 mL NaOH solution (0.1 M) was added and the volume was filled up to 100 mL with double distilled water. Finally, the pH value was adjusted with NaOH solution (0.1 M) or HCl solution (0.1 M).

Glycine/NaOH buffer (5 mM, pH = 9, I = 10 mM). The buffer was prepared by dissolving 37.53 mg glycine and 52.35 mg NaCl in approximately 70 mL double distilled water. Afterwards, 1.041 mL NaOH solution (0.1 M) was added and the volume was filled up to 100 mL with double distilled water. Finally, the pH value was adjusted with NaOH solution (0.1 M) or HCl solution (0.1 M).

Buckling experiments. Buckling experiments were performed on neutral and charged hollow microgels by increasing the osmotic pressure of the medium using dextran (Alfa Aesar, $M_\mathrm{w} \approx 150\,000$ g mol^{-1}) as a free polymer. The osmotic pressure of the dextran solution π can be calculated from the weight percentage of the solution β as: $\pi_{\mathrm{Dextran}\,150\,000} = 286\beta + 87\beta^2 + 5\beta^3$ for $0.2 < \beta < 15$.[55] Stock solutions of Dextran 150 000 of concentration 20 wt% were prepared in Milli-Q water and buffer solutions of pH = 3 and 9. All the buckling experiments were performed at a Dextran concentration of 10 wt% which corresponds to an osmotic pressure of ≈16.5 kPa[52,55] and the microgel concentrations of 2.3×10^{-3} and 2.6×10^{-3} wt% for the PNIPAM and P(NIPAM-*co*-DMI) hollow microgels, respectively. To quench the charged hollow microgels at different pH, a solution of hollow microgels, 10 wt% Dextran, and 1 mM NaOH (pH = 11) was prepared. After 1 hour, HCl (2 mM) was added to the same solution to reduce the pH up to 3. Finally, again after 1 hour, 2 mM NaOH was added to increase the pH to 11. The fraction of buckled particles f_B was estimated by counting the number of individual buckled and spherical particles based on more than 100 microgels.

1.1 Methods

Scanning electron microscopy (SEM). SEM measurements were performed to calculate the size and polydispersity of the silica particles. Moreover, SEM measurements were performed to test the full core removal. The diluted sample solutions were dried on clean silicon wafers and investigated by means of FE-SEM (LEO/Zeiss Supra 35 VP).

Fluorescence microscopy (FM). Fluorescence microscopy experiments were conducted using an inverted fluorescence microscope (TE300 Nikon), that was equipped with a Blackfly S BFS-U3-04S2M camera. Two objectives, Nikon plan fluoro oil NA 0.5–1.3 objective with a magnification of 100× and a Nikon Plan Apo NA 0.95 objective with a magnification of 40×, were used. For all the fluorescence microscopy techniques, the dispersions (8 μL) were hermetically sealed between two cover glasses separated using a 120 μm spacer with a 51 mm aperture (SecureSeal Imaging). To control the sample temperature, a thermostated enclosure from Okolab was utilized, which leads to a temperature accuracy of less than 0.1 °C. Each sample (with a concentration of 0.0035 wt%) was examined at 20 °C. The software ImageJ was used to analyze the micrographs.

Spinning disk fluorescence microscopy (SDFM). SDFM measurements were performed using an inverted epifluorescence microscope (Nikon Eclipse TI: HUBC/A). The microscope was equipped with a 100× oil immersion objective (Nikon HP Plan

Apo VC, NA = 1.40) and a beam splitter (Semrock Di01-T405/488/568/647 quad-band dichroic mirror). SDFM was enabled by a spinning disk (Yokogawa CSU-X1FW) with a spinning frequency of 5000 rpm. A 488 nm laser (Toptica iBeam smart 488S-HP) with a theoretical maximal power of 200 mW was used to excite FITC and a 561 nm laser (Cobolt Jive TEM) with theoretical maximal power of 500 mW was used to excite Rhodamine B. A *xyz*-piezo stage was used to move the measuring cells with the precision of a few nanometers. The micrographs were recorded with a EMCCD (Andor iXon Ultra) with 1024 × 1024 px, electron multiplier mode and a camera pixel size of 13 μm px^{-1}. The 100× magnification by the objective lens and an additional magnification of 1.2× causes a final image pixel size of 108.33 nm px^{-1}. For all images, the EM-Gain was set to a value of 1. Laser intensity and exposure times were adjusted depending on the detected intensity. Generally, for the imaging of static objects, *e.g.* interfaces or particles adsorbed to the cover glass, a higher exposure time of 130 ms and lower laser intensities were chosen in comparison to the imaging of dynamic objects, *e.g.*, particles in the bulk, whereby lower exposure times in the range 20 to 50 ms and higher laser intensities were selected. The processing of the micrographs was performed with the software ImageJ.

Confocal laser scanning microscopy (CLSM). The hollow PNIPAM microgels and P(NIPAM-*co*-IA) microgels at pH = 9 were imaged with a Leica SP5 operated in the inverted mode (D6000I), using a 100×/1.4 NA immersion objective. A constant temperature of 25 °C was ensured by a thermostated enclosure (life Imaging Service). A 543 nm HeNe laser was used to excite the red fluorescence of rhodamine B. The suspensions (≈ 8 μL) were hermetically sealed between two untreated cover glasses separated by a 120 μm spacer with a 51 mm aperture (SecureSeal Imaging). Buckling experiments were performed with the same setup either in FM or CLSM modes at room temperature (22 °C).

Atomic force microscopy (AFM). AFM measurements were performed on a Dimension Icon AFM with a closed loop (Veeco Instruments Inc., software Nanoscope 9.4 (Bruker Corporation)). Acquired data was processed using Nanoscope Analysis and Gwyddion. The core–shell silica/PNIPAM and silica/P(NIPAM-*co*-IA) microgels and their corresponding hollow PNIPAM and P(NIPAM-*co*-IA) capsules were deposited onto a glass slide either by spin-coating or drop casting. At first, glass coverslips with a size of 2.2 × 2.2 cm (Menzel-Gläser, n4) were cleaned by ultrasonication in isopropanol for 15 min. Then the glass surface was activated by UV ozone treatment (Nanobioanalytics UVC-1014) for 15 min. Finally, the pre-cooled microgel solution (water for PNIPAM based and pH = 9 buffer for PNIPAM-*co*-IA based microgels) with a concentration 0.01 wt% were added onto the glass slides. The samples were either spin-coated (Convac 1001S) at a speed of 2500 rpm for 30 s or drop casted at room temperature. The configuration of the microgels at the air/glass interface was investigated in the dried state in tapping mode using OTESPA tips with a resonance frequency of 300 kHz, a nominal cantilever spring constant of 26 Nm^{-1}, and a nominal tip radius of <7 nm (NanoAndMore GmbH, Germany).

Dynamic light scattering (DLS). Dynamic light scattering experiments were conducted using an ALV-setup equipped with a HeNe laser light source with a wavelength of λ = 633 nm. It included a goniometer (ALV/CGS-8F), two avalanche photodiodes (PerkinElmer Inc. SPCM-CD2969), a digital hardware correlator (ALV 5000) and light scattering electronic (ALV/LSE-5003). To ensure free diffusion and measurements without multiple scattering, the samples were diluted at 3.3×10^{-3} wt%. PNIPAM microgel capsules were dispersed in double distilled water and P(NIPAM-*co*-DMI) capsules in glycine/HCl buffer (5 mM, I = 1 mM) at pH = 3 and pH = 9. The measurements were performed at scattering angles θ ranging from 30 to 70° in 10° steps, which corresponds to a variation of the scattering wave vector $q = (4\pi n/\lambda)\sin(\theta/2)$ from *circa* 7×10^{-3} to $1.5 \times 10^{-2}\ \text{nm}^{-1}$, where n is the refractive index of the solvent. The silica particles were measured in EtOH at 20 °C, whereas the microgel capsules were measured in water from 20 °C to 41 °C in steps of 3 °C. The initial decay rate Γ was derived from a first-order cumulant analysis of the normalized intermediate scattering function $f(q,t)$. The diffusion coefficient D was estimated from the q^2-dependence $\Gamma = Dq^2$, and the hydrodynamic radius R_H was obtained *via* the Stokes–Einstein relationship $D = k_\text{B}T/(6\pi\eta_\text{s}R_\text{H})$, where k_B, η_s, and T are the Boltzmann constant, solvent viscosity, and absolute temperature, respectively.[56]

Static light scattering (SLS). SLS measurements were conducted using a closed goniometer from SLS-Systemtechnik equipped with different lasers. The goniometer was connected to a thermostat (Julabo CF40) to control the sample temperature which is surrounded by a toluene bath. The samples were highly diluted to ensure free diffusion and to avoid multiple scattering. The scattered intensity was measured for scattering angles from 15° to 150° in steps of 1°. The silica particles were investigated in EtOH at 20 °C using a 640 nm laser. The microgel capsules were measured in aqueous solution at 20 °C and 40 °C using the lasers of 407 nm, 640 nm, and 819 nm for a broader q-range. The scattering data were evaluated using the Matlab-based software FitIt!.‡[57] The silica particles were fitted using a hard-sphere model[58] and the hollow particles were fitted using a fuzzy-core–shell model introduced by Berndt *et al.*[59]

Differential dynamic microscopy (DDM). The DDM measurements were performed by using an inverted epifluorescence microscope (Nikon Eclipse TE300) with bright field illumination. The microscope was equipped with a 40× objective (Nikon CFI P-Apo Lambda, NA = 0.95). The data were recorded with a camera (Blackfly S BFS-U3-04S2M) with a pixel size of 175.26 nm. For each sample, seven videos with 10 000 frames and a frame rate of 500 Hz were recorded. Diluted samples were temperature-controlled using an Okolab incubation unit, adjusting temperatures from 20 °C to 40 °C in 5 °C intervals with a temperature sensor near the sample. The data were

---

‡ https://github.com/ovirtanen/fitit

evaluated with the software DDMSoft.§[52] We refer readers to the ESI† for further details on the data evaluation.

Electrophoretic mobility measurements. Measurements of the ζ-potentials and of the electrophoretic mobility were performed by using a Litesizer (Anton Paar). All measurements were performed at 20 °C by using a 658 nm single-frequency laser diode. The electrophoretic mobility of P(NIPAM-*co*-IA) capsules was investigated in aqueous buffer solutions. For calculation of the ζ-potential, the Smoluchowski's equation was used. Each value was averaged over 100 to 1000 runs, whereby the measurements were stopped when the standard deviation was less than 1 mV.

2 Results and discussion

The radius of fluorescent-labelled silica seeds was determined *via* SLS and DLS (refer to Fig. S1, ESI†) at 179 nm and 178 nm, respectively.[60] These small, labelled silica seeds were further used for the synthesis of the micro-sized silica-core particles. The SEM analysis confirmed the low size polydispersity (4%) of the core-particles with a mean radius determined from statistical analysis of 50 particles at 530 ± 3 nm as shown in Fig. 2A. After surface functionalization, either a PNIPAM or P(NIPAM-*co*-IA) microgel shell was synthesized.

Confocal fluorescence images of the core–shell silica/P(NIPAM) and silica/P(NIPAM-*co*-IA) microgels in dispersion are presented in Fig. 2B and C confirming the successful synthesis procedure due to the clear identification of core and shell. AFM measurements performed on the two systems in the dried state (see Fig. S2, ESI†) further confirm the presence of the core with a maximal height slightly higher than 1000 nm for both systems in the order of the silica core diameter. Both systems are also characterized by limited spreading at the surface evidenced by an average diameter in the order of 1200 and 1300 nm for the neutral and charged core–shell microgels, respectively. In this case the evaluation is limited by the topography of the particles which prevents clear imaging of the adsorbed corona close to the silica core.

The cores of the two core–shell systems were subsequently dissolved in NaOH solution to yield hollow microgel capsules, as outlined in the synthesis section. We first investigate the dried capsules *via* confocal and AFM imaging. A dramatic change in the microstructure could be observed in comparison to the core–shell systems. Although individual objects can be observed, the resulting particles at the glass surface are highly deformed and present a buckled and wrinkled conformation characteristic of collapsed soft capsules as shown from the AFM height imaging in the dried state of drop casted samples in Fig. 3. The microgel capsule contact areas, which are mostly circular, exhibit large variations in diameter ranging from approximately 1 to 3.5 μm, and are by far exceeding the diameters of the core–shell systems. The neutral hollow microgels spread and flatten at the substrate adopting either a wrinkled conformation characterized by a lower diameter or a fully adsorbed conformation (Fig. 3A–C). Their average size is almost two times smaller than their charged counterparts, which is also reflected by their height profiles. In comparison, for the charged hollow microgels we could even observe very large and thin and sometimes partially disrupted systems that could correspond to ruptured capsules (Fig. 3D–F). From the difference between height profiles, we could assume that after adsorption and drying neutral microgels maintain capsule integrity. The large spreading of the charged microgel capsules can further be rationalized by their softness and the strong repulsive electrostatic interactions of their shell with the negatively charged ozone treated substrate. Two sample preparations, *i.e.*, drop casting and spin-coating, performed on hydrophilic glass substrates were compared. Spin-coating the samples results in a lower distribution of diameters, however much fewer objects could be detected on a single micrograph, resulting so far in rather poor statistics based on seven capsules. Characteristic AFM height micrographs of spin-coated neutral and charged capsules are shown in Fig. S3A and B (ESI†) together with their average height profiles in Fig. S3C (ESI†). The mean diameter estimated from this analysis was 1820 ± 320 nm and 3400 ± 300 nm for the neutral and charged microgels, respectively. The corresponding average heights were measured at 21 ± 5 nm and 6.0 ± 1.3 nm. Comparing

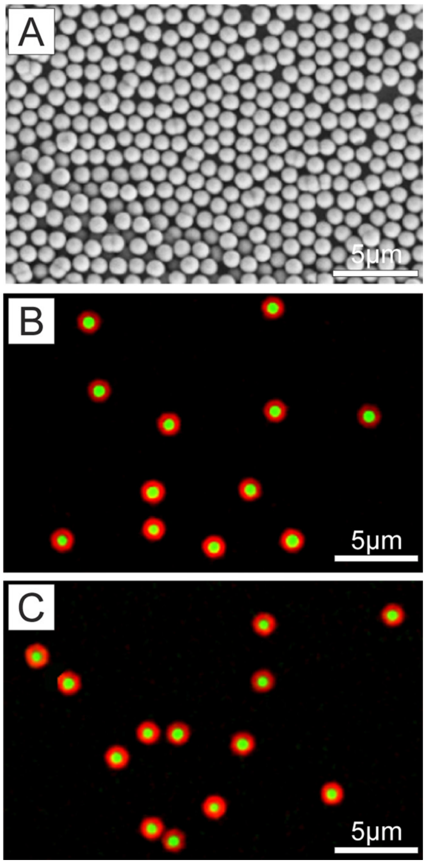

Fig. 2 (A) Scanning electron micrographs of the silica core-particles. (B) Confocal fluorescence micrographs of the core–shell PNIPAM and (C) P(NIPAM-*co*-IA) particles in dispersion, Scale bars: 5 μm.

---

§ https://github.com/duxfrederic/ddmsoft

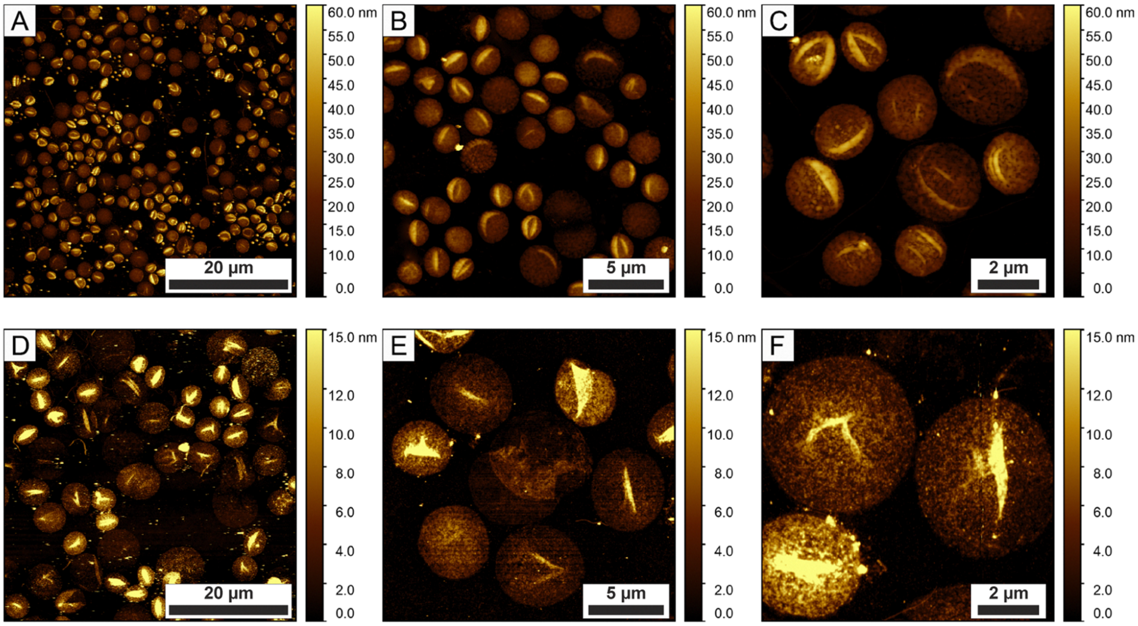

Fig. 3 AFM height micrographs of the neutral PNIPAM ($50 \times 50\ \mu m^2$, $20 \times 20\ \mu m^2$, $10 \times 10\ \mu m^2$) (A)–(C) and charged P(NIPAM-*co*-IA, pH = 9) ($50 \times 50\ \mu m^2$, $20 \times 20\ \mu m^2$, $10 \times 10\ \mu m^2$, zoom in) (D)–(F) capsules respectively. Measurements were performed under dry conditions after drop casting using the tapping mode.

the average height and diameter of spin-coated and drop casted microgel capsules in Fig. S3D (ESI†), we observed that the squared radius scales with height, which would indicate the dried microgel volume (assuming a disk geometry) is almost the same for all capsules, *i.e.*, that both the neutral and charged capsules are monodisperse and have the same mass. We further investigate their swollen conformation when adsorbed at untreated glass using CLSM (Fig. 4). The majority of the systems appear as hollow capsules with the presence of a large cavity confirmed by 3D reconstruction from *z*-stack imaging (Fig. 4E–H). These systems coexist with microgels strongly deformed at the glass. In addition, due to their extreme softness and their adhesion to the glass surface, some of the hollow charged microgels become strongly deformed along the shear created during the sample preparation as shown in Fig. 4B, D and F.

Having characterized the structure of both hollow microgel capsules at surfaces both in their dried and swollen state, we further investigate their behaviour in dispersion in their swollen state. The fluorescence imaging of both hollow microgel capsules with a concentration about $c \approx 0.003$ wt% is shown in Fig. 5. The neutral microgel capsules were dispersed in Milli-Q water (Video S1, ESI†), whereas the charged microgel capsules were first investigated in buffer at pH = 9 (Video S2, ESI†) at 20 °C. Fluorescence imaging evidences the good dispersion of both systems, that appear well-defined and the presence of the cavity surrounded by the fluorescent microgel shell. When both microgel capsules appear in the majority rather than monodisperse in size and shape, we noted that charged hollow microgel capsules were more polydisperse with several particles presenting an irregular shape (see Fig. 5B and Video S2, ESI†). Strikingly, not only do the charged microgels appear significantly larger, but also much softer as characterized by thermal shape fluctuations that could be evidenced *via* CLSM measurements performed at 25 °C (Video S3, ESI†).

We then turn our attention to the responsivity of the microgel capsules starting with the neutral microgel system. To explore the temperature responsiveness outlined in Fig. 6A, we initiated our investigation by systematically conducting DLS on the diluted neutral PNIPAM capsules. When performing such measurements for large particles, one should be aware that the calculated diffusion may be presenting a large q-dependence around minima of the particle form factor. An example of the first-cumulant analysis of the $f(q,\tau)$ measured at 20 °C is provided in the ESI† (Fig. S6A). The analysis was therefore performed on the available q-range and the diffusion coefficient defined as the average diffusion over all angles. This was motivated by the large dimensions of the investigated systems. As DLS is influenced by the form factor of the particles large variation of the measured hydrodynamic radius are expected for scattering angles in the vicinity of the form factor minima.[61,62] In addition, an additional relaxation mode may be related to shape fluctuations as observed for instance in the case of lipid vesicles (see the ESI† for further details).[63] As the low q region is limited, we therefore decided to average over the whole q-range. The swelling curves were measured first with increasing temperature and then by decreasing temperature to check the reversibility of the response. PNIPAM capsules show the typical behaviour expected from conventional PNIPAM microgels with a slightly higher VPTT around 33–34 °C (Fig. 6B). In their swollen state at 20 °C and collapsed state at 41 °C, R_H was determined at 837 nm and 531 nm, respectively.

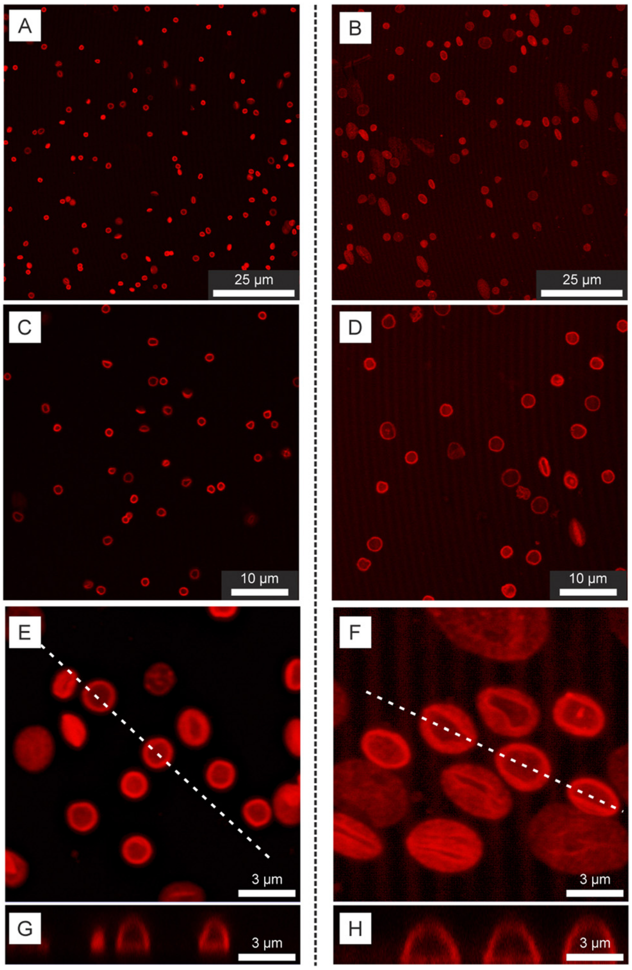

Fig. 4 CLSM micrographs of swollen neutral and charged microgel capsules adsorbed at the glass coverslip. (A)–(D) 2D micrographs captured at different magnifications of the neutral (A) and (C) and charged (B) and (D) microgel capsules. (E) and (F) Maximum intensity projections of the neutral (E) and charged systems obtained from 3.02 µm thick z-stacks. The dashed lines indicate the cross-sections shown in (G) and (H).

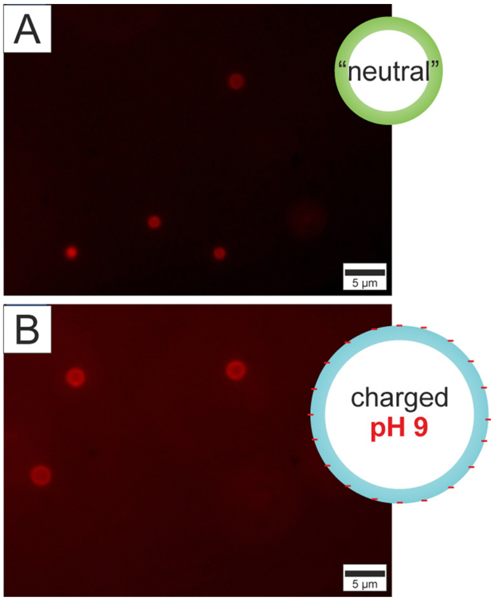

Fig. 5 Fluorescence imaging of neutral hollow PNIPAM capsules dispersed in pure Milli-Q (A) and charged hollow P(NIPAM-*co*-IA) capsules in pH = 9 buffer (B) at 20 °C together with a schematic representation of their respective conformation. Scale bars: 5 µm.

In addition, SLS measurements were performed under similar conditions to some further insights into the conformation of the capsules. The measurements were conducted at 20 and 40 °C and as shown in Fig. 6C. The form factor measured at 20 °C is well resolved with many maxima confirming the narrow size and conformation distribution of the capsules.[52,64] At 40 °C, the maxima and minima become more pronounced and shift to higher q-values indicating the decrease of the capsule size, thickness and fuzziness. Fits with a fuzzy capsule model appropriately capture the main scattering features at the exception of the more smeared out first minimum in the experiments. The corresponding normalized polymer density profiles are shown in Fig. 6D. The obtained dimensions of the overall capsule radius are in good agreement with the DLS measurements. In addition, the size polydispersity derived from the fits was found to decrease from 11.5 to 6.0%.

The responsivity of the ionic P(NIPAM-*co*-IA) capsules to ionic strength, pH and temperature schematically displayed in Fig. 7A was further investigated. To test the weak polyelectrolyte properties of the P(NIPAM-*co*-IA) capsules, confocal spinning disk fluorescence microscopy (SDFM) measurements were conducted in aqueous buffer solution. The dimensions of the capsules were determined at pH = 3 (I = 10 mM) (Fig. 7A) and pH = 9 (I = 10 mM) (Fig. 7B) from the intensity profiles captured in the equatorial plane. The evaluation of 25 capsules at pH = 3 gives a mean radius of 0.69 ± 0.02 µm and the measurement of 25 capsules at pH = 9 gives a mean radius of 0.94 ± 0.02 µm. Electrophoretic mobility measurements were performed in a buffer with a fixed ionic strength concentration of 10 mM at 20 °C. The ζ-potential is a theoretical quantity and defined for hard particles. However, it loses its physical meaning for soft particles such as microgels and electrophoretic mobility is alternatively used as a quantity that provides information about the surface charge.[65,66] The mean electrophoretic mobility was determined at pH = 3 at $(0.11 \pm 0.03) \times 10^{8}\ \mathrm{m^2\ V^{-1}\ s^{-1}}$ and at pH = 9 at $(-1.11 \pm 0.02) \times 10^{8}\ \mathrm{m^2\ V^{-1}\ s^{-1}}$. The measurements clearly show the ionization of the capsules, which leads to a negative charge at pH = 9. Similar results can be found in the literature for small P(NIPAM-*co*-IA) hollow microgels.[50]

Suggesting a two-stage deprotonation with increasing pH-values corresponding to the step-by-step deprotonation of the two acid groups ($-\mathrm{COOCH_3}$) in the IA moiety. It was found that the P(NIPAM-*co*-IA) microgels are mainly protonated at pH = 3 and fully deprotonated at pH = 9.[50] The observed change in size when the pH value increases from 3 to 9 can be attributed to the charges in the microgels. At a low pH value (pH = 3), two acidic groups ($-\mathrm{COOCH_3}$) are fully neutralized through protonation, facilitating the formation of hydrogen bonds with the amide

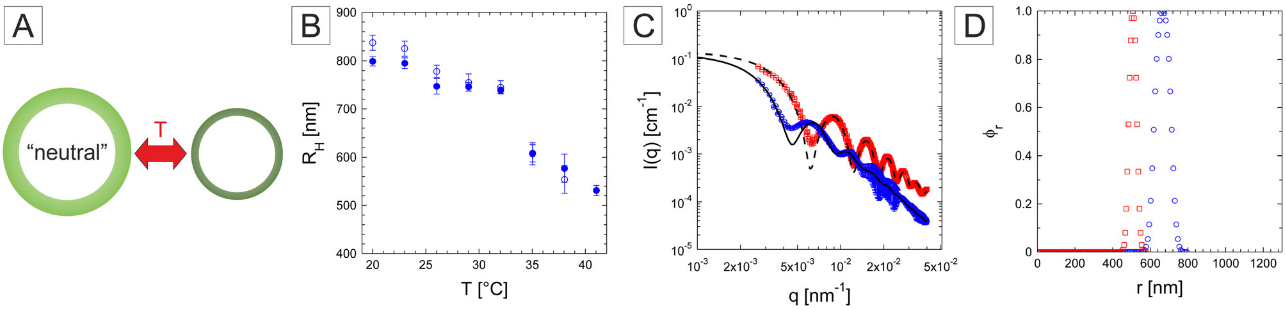

Fig. 6 (A) Schematic swelling behaviour of the neutral PNIPAM capsules, (B) swelling behaviour of the neutral PNIPAM microgel capsules probed by DLS. The hydrodynamic radius was measured with increasing (full symbols) and decreasing temperature (hollow symbols). (C) Form factor of the capsules measured at 20 °C (blue circles) and 40 °C (red squares) fitted with a fuzzy core–shell model (full and dashed lines). (D) Relative radial density profile obtained from fits at 20 °C (blue circles) and 40 °C (red squares).

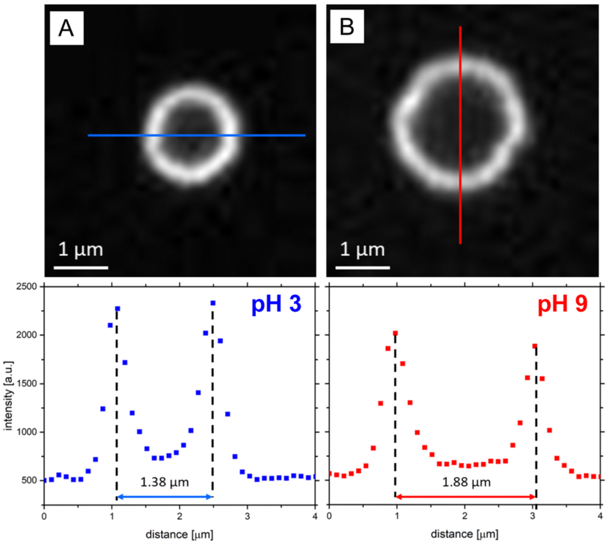

Fig. 7 Confocal spinning disk fluorescence microscopy (SDFM) images (top) and associated intensity profiles (below) of P(NIPAM-*co*-IA) capsules in aqueous solution at pH = 3, *I* = 10 mM (A) and pH = 9, *I* = 10 mM (B).

(–CONH) groups of PNIPAM rather than relying on electrostatic interactions.[67] At pH = 9, the presence of deprotonated acidic groups does not favour the formation of similar hydrogen bonds. Counterions are located in the surrounding of fixed charges but are still mobile for entropic reasons and create an osmotic pressure between the network and solution. Thus, the network swells. In addition, electrostatic repulsion works between the fixed charges, which tend towards the periphery of the capsules and pull the network outwards until expansion is compensated by elastic forces.[50]

The thermoresponsivity of the P(NIPAM-*co*-IA) microgels was first tested at fixed ionic strength (I = 10 mM) *via* DDM (see Fig. S4 and S5 and the ESI† for further details). At pH = 9, the P(NIPAM-*co*-IA) capsules are swollen with a constant $R_H \approx$ 950 nm (see Fig. S5B, ESI†) up to 40 °C. However, the P(NIPAM-*co*-IA) capsules at pH = 3 become responsive to temperature in their protonated state and their size (R_H) decreases from about 750 nm at 20 °C to 500 nm at 35 °C (see Fig. S5A, ESI†) before the capsule dispersion become unstable at higher temperatures.[50] In their collapsed state the protonated capsules are only electrostatically stabilized by residual initiator fragments that are screened by the high ionic strength of the solution leading to the coagulation of the capsules. Note that the ionic strength also seems to play a role at pH = 9, leading to moderate deswelling from 10 to 100 mM buffer by screening the electrostatic repulsion between the deprotonated network moieties.

To minimize this effect, we performed DLS measurements under highly dilute conditions with a 10 mM buffer without adding any extra NaCl salt. The P(NIPAM-*co*-IA) capsules at pH = 9 did not show any temperature dependence similarly to the DDM results, with however a larger radius determined around 1.3 µm (Fig. 8C). Examples of the fitted $f(q,\tau)$ for both pH conditions measured at 20 °C are provided in Fig. S6 (ESI†). The large error bars are here a consequence of the large variation observed in the determination of D at the different angles, which could be related to the form factor of the capsules and to the larger polydispersity and fluctuations of the capsules in size and shape. We note that this value is significantly larger than the DDM measurements performed with the addition of NaCl. Measurements at pH = 3 (Fig. 8D) confirmed the response in temperature with a large size reduction from 941 nm to 296 nm above the VPTT also detected around 33–34 °C pointing to the complete collapse of the capsules. Interestingly, unlike the other systems, the response is not reversible and the measured radius by decreasing temperature became significantly smaller than the initial recorded values below the VPTT.

The SLS analysis was applied to the P(NIPAM-*co*-IA) capsules at pH = 9, and the measurements at the two temperatures are almost similar confirming that the capsules do not respond significantly to temperature in this temperature range (see Fig. 8E). The data could be fitted with a similar model leading to an overall size of about 1.21 and 1.16 µm and shell thickness of *circa* 211 and 167 nm at 20 and 40 °C, respectively (Fig. 8F). The corresponding polydispersity was derived at 20 °C and 13.9%. Note that the large dimensions of the capsules do not allow us to probe the forward scattering affecting the robustness

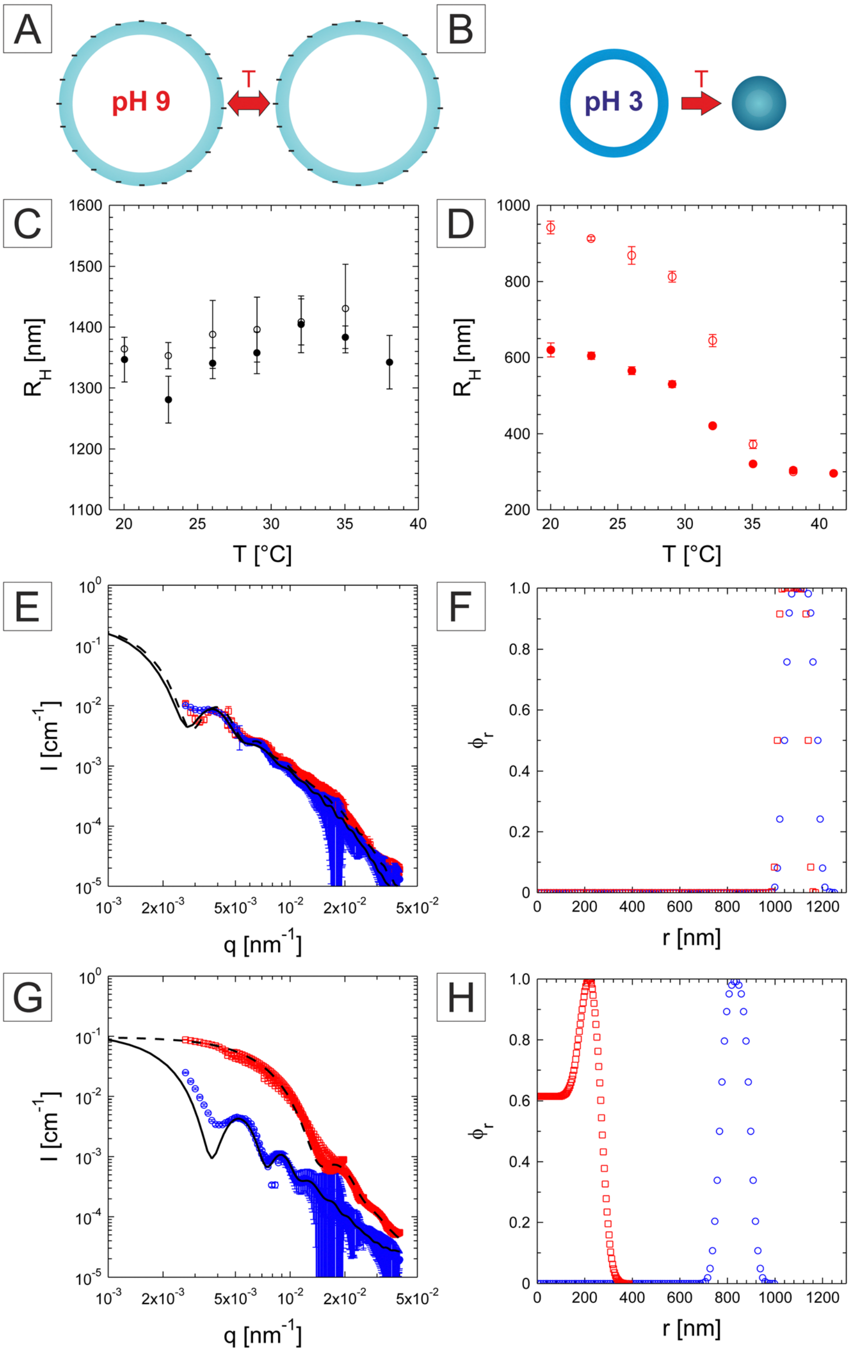

Fig. 8 Schematic of the swelling behaviour of P(NIPAM-*co*-IA) capsules at pH = 9 (A) and pH = 3 (B) with temperature. Swelling behaviour of the P(NIPAM-*co*-IA) capsules at pH = 9 (C) and pH = 3 (D) measured by DLS. Hollow symbols correspond to measurements of the hydrodynamic radius first performed with increasing temperature, whereas full symbols correspond to the subsequent measurements with decreasing temperature. (E)–(H) Static light scattering curves and relative radial density profile obtained from the fuzzy-core–shell fit of the P(NIPAM-*co*-IA) capsules at pH = 9 (E), (F) and pH = 3 (G), (H) at 20 °C (blue circles) and 40 °C (red squares).

of the fits. Finally, the SLS measurements performed at pH = 3 support the size reduction and the formation of more defined capsules characterized by better defined minima and maxima at 20 °C (Fig. 8G). The forward scattering could not be fully reproduced by the fit, however, the other features are well described by the analysis. The overall size was derived at 958 nm, which is significantly larger than the DLS results, with a shell thickness of 251 nm (Fig. 8H). The scattering intensity profile changes significantly at 40 °C following the capsule collapse. The data could not be fitted with a simple capsule model anymore pointing to the filling up of the cavity. Similar observations were reported for smaller charged hollow microgels.[50]

In our previous study, it was observed that neutral microgel capsules buckle under sufficient osmotic pressure set by the

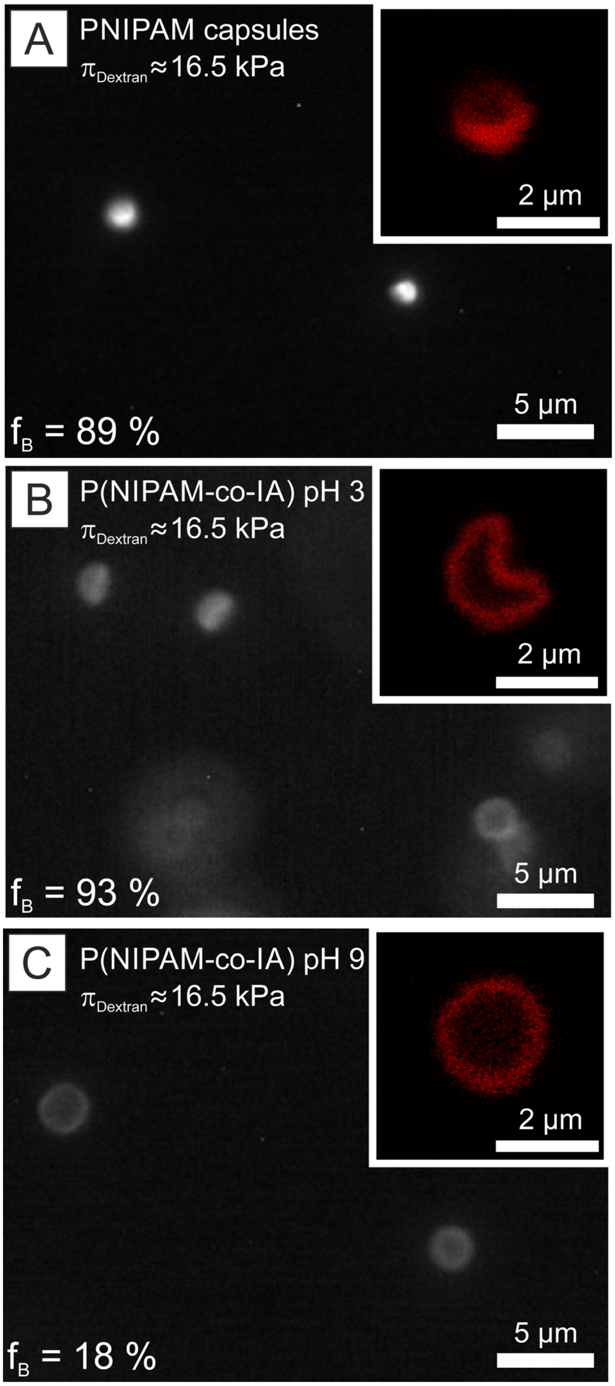

Fig. 9 Microgel capsules under osmotic stress set by the addition of 10 wt% Dextran ($\pi_{Dextran} \approx 16.5$ KPa). Fluorescent micrographs of neutral microgels (A), charged microgels capsules at pH = 3 (B) and charged microgel capsules at pH = 9 (C). The insets show the higher magnification of the capsules recorded under the CLSM imaging mode. The proportion of buckled capsules, f_B, was determined from statistical analysis of the fluorescence micrographs.

addition of high molecular weight Dextran (150 000 g mol^{-1}).[52] This transition is characterized in most of the observations by the development of a single instability leading to a shape transformation from spherical to bowl-shaped. To investigate the influence of charged moieties on the buckling of microgel capsules, dispersions of both neutral and charged capsules were prepared with 10 wt% Dextran, resulting in an osmotic pressure of approximately 16.5 kPa.[52] Experiments on neutral capsules were conducted in pure double distilled water, while charged microgel capsules were dispersed in 1 mM, pH = 9 and 1 mM, pH = 3 buffer solutions. Fluorescence microscopy experiments were performed at 22 °C for the statistical evaluation of the proportion of buckled microcapsules, f_B. Characteristic micrographs are presented in Fig. 9. The analysis was based on the evaluation of more than 100 individual capsules diffusing in solution. Under these conditions, nearly all neutral microcapsules buckle (f_B = 89%) (see Fig. 9A), which is consistent with our previous observations.[52] Similarly, under acidic conditions (Fig. 9B), charged microcapsules predominantly fully buckle (f_B = 93%). Note that in both experiments, we did observe the presence of many aggregates that we ascribe to the onset of depletion interactions.[68,69] Interestingly, as depicted in Fig. 9C, under basic conditions at pH = 9, the majority of the capsules remain spherical (f_B = 18%) and fully dispersed. The additional contribution of electrostatic interactions and the increased osmotic pressure within the microgel network seem to be at the origin of the reduced buckling under these conditions. In addition, pH jump experiments were performed under high osmotic pressure using the same Dextran concentration to check the reversibility of the buckling process with pH (see Fig. S7 and the Experimental section for further details, ESI†). In this case, instead of a buffer solution, the pH of a charged microgel capsule dispersion was adjusted by the addition of sodium hydroxide (NaOH) and hydrochloric acid (HCl). After the addition of 1 mM NaOH, the microgel capsules were mostly unbuckled with f_B = 14% and well dispersed similar to our former observations at pH = 9 (Fig. 9C). Adding 2 mM HCl to the former dispersion, *i.e.*, setting the pH to *circa* pH = 3, the capsules were mostly buckled (f_B = 91%) and aggregated similar to Fig. 9B. Finally, the consecutive addition of 2 mM NaOH, again to the same dispersion, bringing it back to basic conditions was found to result in the unbuckling of the capsule (f_B = 25%) and their redispersion from the aggregates. Such proof of concept experiments clearly establish the versatility of the response of such systems to different stimuli and the possibility for further tuning the conformation, mechanical properties, and eventually the permeability of capsules. A more thorough investigation of the buckling transition of the charged microgel capsules and their kinetics will be undertaken in the future.

3 Conclusion

In this study, well-defined and monodisperse hollow soft microgel capsules were synthesized consisting of a micrometric size range showing temperature and pH responsiveness. The neutral PNIPAM capsules exhibited thermoresponsive behaviour, whereas, the charged P(NIPAM-*co*-IA) capsules were thermoresponsive at low pH (pH = 3) and no temperature responsivity was observed at high pH (pH = 9). The size of the neutral capsules is smaller than the charged capsules and the hollow architecture with extreme softness makes them strongly flatted on glass surfaces. In addition, the hollow responsive microgels were widely characterized using different methods, ranging from direct imaging using confocal, fluorescence, and atomic force microscopy to scattering techniques involving DLS and SLS. The direct imaging confirmed their size range as well as the unique structural behaviour due to softness. The dynamic scattering measurement ensured the temperature-dependent swelling behaviour of PNIPAM and P(NIPAM-*co*-IA) capsules at pH = 3 and the capsule form factor was measured by static light scattering experiments. Moreover, the large swelling of the charged microgel capsules due to very soft behaviour is reflected by thermal fluctuation and high deformability. Both PNIPAM and P(NIPAM-*co*-IA) microgel capsules were found to buckle under a high osmotic pressure of 16.5 kPa. However, while P(NIPAM-*co*-IA) microgel capsules buckle at pH = 3, they remain mostly unbuckled at pH = 10. These initial experiments demonstrate the significance of additional charged moieties in the buckling behaviour. A more systematic investigation of the buckling behaviour and permeability of the P(NIPAM-*co*-IA) microgel capsules, depending on their degree of protonation and ionic strength, will be undertaken in the future. Such a study will further contribute to establishing their application as cargo for nanomaterials transport and delivery. Besides, due to their extreme softness and responsivity toward pH, ionic strength and temperature, they should present some fascinating properties and serve as unique soft model systems to study their assembly at fluid interfaces and their phase behaviour, glass transition and jamming in dispersions at high volume fractions. Hereby, the single particle deformation could be resolved *in situ* in real space with respect to their large dimensions and hollow structure.

Conflicts of interest

There are no conflicts to declare.

Acknowledgements

Financial support from the SFB 985 ''Functional Microgels and Microgel Systems'' of Deutsche Forschungsgemeinschaft is greatly acknowledged. The authors thank the RWTH Start-Up-Grant initiative financed by the Deutsche Forschungsgemeinschaft for the kind support within the project. We would like to thank Rebecca Hengsbach and Prof. Dr Simon from the Institute of Inorganic Chemistry, RWTH Aachen for the SEM measurements and Frédéric Dux for the development of the DDM software.

Notes and references

1 F. A. Plamper and W. Richtering, *Acc. Chem. Res.*, 2017, **50**, 131–140.
2 R. Pelton, *Adv. Colloid Interface Sci.*, 2000, **85**, 1–33.
3 M. Karg, A. Pich, T. Hellweg, T. Hoare, L. A. Lyon, J. Crassous, D. Suzuki, R. A. Gumerov, S. Schneider and I. I. Potemkin, *et al.*, *Langmuir*, 2019, **35**, 6231–6255.
4 B. R. Saunders and B. Vincent, *Adv. Colloid Interface Sci.*, 1999, **80**, 1–25.
5 A. Scotti, M. F. Schulte, C. G. Lopez, J. J. Crassous, S. Bochenek and W. Richtering, *Chem. Rev.*, 2022, **122**, 11675–11700.
6 H. Senff and W. Richtering, *J. Chem. Phys.*, 1999, **111**, 1705–1711.
7 M. Brugnoni, A. C. Nickel, L. C. Kröger, A. Scotti, A. Pich, K. Leonhard and W. Richtering, *Polym. Chem.*, 2019, **10**, 2397–2405.
8 T. Hoare and R. Pelton, *Macromolecules*, 2004, **37**, 2544–2550.
9 M. Karg, I. Pastoriza-Santos, B. Rodriguez-Gonzalez, R. von Klitzing, S. Wellert and T. Hellweg, *Langmuir*, 2008, **24**, 6300–6306.
10 S. Lally, R. Bird, T. J. Freemont and B. R. Saunders, *Colloid Polym. Sci.*, 2009, **287**, 335–343.
11 A. P. Gelissen, A. Scotti, S. K. Turnhoff, C. Janssen, A. Radulescu, A. Pich, A. A. Rudov, I. I. Potemkin and W. Richtering, *Soft Matter*, 2018, **14**, 4287–4299.
12 J. Pinheiro, L. Moura, R. Fokkink and J. Farinha, *Langmuir*, 2012, **28**, 5802–5809.
13 E. Daly and B. R. Saunders, *Langmuir*, 2000, **16**, 5546–5552.
14 D. Kleinschmidt, K. Nothdurft, M. V. Anakhov, A. A. Meyer, M. Mork, R. A. Gumerov, I. I. Potemkin, W. Richtering and A. Pich, *Mater. Adv.*, 2020, **1**, 2983–2993.
15 M. Barth, M. Wiese, W. Ogieglo, D. Go, A. J. Kuehne and M. Wessling, *J. Membr. Sci.*, 2018, **555**, 473–482.
16 L. V. Sigolaeva, S. Y. Gladyr, A. P. Gelissen, O. Mergel, D. V. Pergushov, I. N. Kurochkin, F. A. Plamper and W. Richtering, *Biomacromolecules*, 2014, **15**, 3735–3745.
17 D. Buenger, F. Topuz and J. Groll, *Prog. Polym. Sci.*, 2012, **37**, 1678–1719.
18 D. Keskin, O. Mergel, H. C. Van der Mei, H. J. Busscher and P. van Rijn, *Biomacromolecules*, 2018, **20**, 243–253.
19 M. Dirksen, C. Dargel, L. Meier, T. Brändel and T. Hellweg, *Colloid Polym. Sci.*, 2020, **298**, 505–518.
20 R. Dave, G. Randhawa, D. Kim, M. Simpson and T. Hoare, *Mol. Pharmaceutics*, 2022, **19**, 1704–1721.
21 N. M. Smeets and T. Hoare, *J. Polym. Sci., Part A: Polym. Chem.*, 2013, **51**, 3027–3043.
22 D. Klinger and K. Landfester, *Polymer*, 2012, **53**, 5209–5231.
23 Y. Hertle and T. Hellweg, *J. Mater. Chem. B*, 2013, **1**, 5874–5885.
24 J. Oberdisse and T. Hellweg, *Colloid Polym. Sci.*, 2020, **298**, 921–935.
25 S. Nayak, D. J. Gan, M. J. Serpe and L. Lyon, *Small*, 2005, **1**, 416–421.
26 H. Gao, W. Yang, K. Min, L. Zha, C. Wang and S. Fu, *Polymer*, 2005, **46**, 1087–1093.
27 J. Dubbert, T. Honold, J. S. Pedersen, A. Radulescu, M. Drechsler, M. Karg and W. Richtering, *Macromolecules*, 2014, **47**, 8700–8708.

28 A. Scotti, M. Brugnoni, A. A. Rudov, J. E. Houston, I. I. Potemkin and W. Richtering, *J. Chem. Phys.*, 2018, **148**, 174903.

29 K. C. Bentz and D. A. Savin, *Polym. Chem.*, 2018, **9**, 2059–2081.

30 Y. Su, O. F. Ojo, I. K. M. Tsengam, J. He, G. L. McPherson, V. T. John and J. A. Valla, *Langmuir*, 2018, **34**, 14608–14616.

31 L. Zha, Y. Zhang, W. Yang and S. Fu, *Adv. Mater.*, 2002, **14**, 1090–1092.

32 M. Windbergs, Y. Zhao, J. Heyman and D. A. Weitz, *J. Am. Chem. Soc.*, 2013, **135**, 7933–7937.

33 S. K. Wypysek, S. P. Centeno, T. Gronemann, D. Wöll and W. Richtering, *Macromol. Biosci.*, 2023, 2200456.

34 M. Deloney, K. Smart, B. A. Christiansen and A. Panitch, *J. Controlled Release*, 2020, **323**, 47–58.

35 A. J. Schmid, J. Dubbert, A. A. Rudov, J. S. Pedersen, P. Lindner, M. Karg, I. I. Potemkin and W. Richtering, *Sci. Rep.*, 2016, **6**, 22736.

36 H. Masoud and A. Alexeev, *ACS Nano*, 2012, **6**, 212–219.

37 A. Moncho-Jorda, A. Germán-Bellod, S. Angioletti-Uberti, I. Adroher-Bentez and J. Dzubiella, *ACS Nano*, 2019, **13**, 1603–1616.

38 S. Seiffert, J. Thiele, A. R. Abate and D. A. Weitz, *J. Am. Chem. Soc.*, 2010, **132**, 6606–6609.

39 W. Xu, A. A. Rudov, R. Schroeder, I. V. Portnov, W. Richtering, I. I. Potemkin and A. Pich, *Biomacromolecules*, 2019, **20**, 1578–1591.

40 Z. Li, M.-H. Kwok and T. Ngai, *Macromol. Rapid Commun.*, 2012, **33**, 419–425.

41 M. Horecha, V. Senkovskyy, M. Stamm and A. Kiriy, *Macromolecules*, 2009, **42**, 5811–5817.

42 Q. Sun and Y. Deng, *J. Am. Chem. Soc.*, 2005, **127**, 8274–8275.

43 Z. Cao, U. Ziener and K. Landfester, *Macromolecules*, 2010, **43**, 6353–6360.

44 F. Lu, Y. Luo, B. Li, Q. Zhao and F. J. Schork, *Macromolecules*, 2010, **43**, 568–571.

45 C.-J. Huang and F.-C. Chang, *Macromolecules*, 2009, **42**, 5155–5166.

46 J. Vialetto, F. Camerin, F. Grillo, S. N. Ramakrishna, L. Rovigatti, E. Zaccarelli and L. Isa, *ACS Nano*, 2021, **15**, 13105–13117.

47 V. Lapeyre, N. Renaudie, J.-F. Dechezelles, H. Saadaoui, S. Ravaine and V. Ravaine, *Langmuir*, 2009, **25**, 4659–4667.

48 J. Dubbert, K. Nothdurft, M. Karg and W. Richtering, *Macromol. Rapid Commun.*, 2015, **36**, 159–164.

49 M. Brugnoni, F. Fink, A. Scotti and W. Richtering, *Colloid Polym. Sci.*, 2020, **298**, 1179–1185.

50 S. K. Wypysek, A. Scotti, M. O. Alziyadi, I. I. Potemkin, A. R. Denton and W. Richtering, *Macromol. Rapid Commun.*, 2020, **41**, 1900422.

51 M. P. Neubauer, M. Poehlmann and A. Fery, *Adv. Colloid Interface Sci.*, 2014, **207**, 65–80.

52 F. Hagemans, F. Camerin, N. Hazra, J. Lammertz, F. Dux, G. Del Monte, O.-V. Laukkanen, J. J. Crassous, E. Zaccarelli and W. Richtering, *ACS Nano*, 2023, **17**, 7257–7271.

53 C. Gao, E. Donath, S. Moya, V. Dudnik and H. Möhwald, *Eur. Phys. J. E: Soft Matter Biol. Phys.*, 2001, **5**, 21–27.

54 W. Stöber, A. Fink and E. Bohn, *J. Colloid Interface Sci.*, 1968, **26**, 62–69.

55 C. Bonnet-Gonnet, L. Belloni and B. Cabane, *Langmuir*, 1994, **10**, 4012–4021.

56 W. Burchard and W. Richtering, *Progr. Colloid Polym. Sci.*, 1989, **80**, 151–163.

57 O. L. J. Virtanen, PhD thesis, RWTH Aachen University, 2016, pp. 1–186.

58 A. Van Helden and A. Vrij, *J. Colloid Interface Sci.*, 1980, **78**, 312–329.

59 I. Berndt, J. S. Pedersen and W. Richtering, *J. Am. Chem. Soc.*, 2005, **127**, 9372–9373.

60 W. Burchard, *Light scattering from polymers*, 1983, pp. 1–124.

61 W. Van Megen and P. Pusey, *Phys. Rev. A: At., Mol., Opt. Phys.*, 1991, **43**, 5429.

62 G. Bryant, S. Martin, A. Budi and W. van Megen, *Langmuir*, 2003, **19**, 616–621.

63 P. Brocca, L. Cantù, M. Corti, E. Del Favero and S. Motta, *Langmuir*, 2004, **20**, 2141–2148.

64 J. Park, E. Lee, N.-M. Hwang, M. Kang, S. C. Kim, Y. Hwang, J.-G. Park, H.-J. Noh, J.-Y. Kim and J.-H. Park, *et al.*, *Angew. Chem.*, 2005, **117**, 2932–2937.

65 H. Ohshima, *Colloid Polym. Sci.*, 2007, **285**, 1411–1421.

66 H. Ohshima, *Electrophoresis*, 1995, **16**, 1360–1363.

67 V. Nigro, R. Angelini, B. Rosi, M. Bertoldo, E. Buratti, S. Casciardi, S. Sennato and B. Ruzicka, *J. Colloid Interface Sci.*, 2019, **545**, 210–219.

68 P. Jenkins and M. Snowden, *Adv. Colloid Interface Sci.*, 1996, **68**, 57–96.

69 H. N. W. Lekkerkerker, R. Tuinier and M. Vis, *Depletion Interaction*, Springer International Publishing, Cham, 2024, pp. 67–120.